DOI: https://doi.org/10.62985/j.huit_ojs.vol25.noS1_ICA.285

EFFECT OF CALCINATION TEMPERATURE ON THE SYNTHESIS OF TiO_2-SiO_2 COMPOSITES AND THEIR PHENOL DEGRADATION PERFORMANCE

Thi Ngoc Suong Ho*

Ho Chi Minh City University of Industry and Trade

*Email: *suonghtn@huit.edu.vn*

Received: 2 May 2025; Revised: 22 May 2025; Accepted: 1 June 2025

ABSTRACT

This study investigates the effect of calcination temperature on the synthesis of TiO_2-SiO_2 composites and evaluates their efficiency in degrading phenol from aqueous solutions. The TiO_2-SiO_2 composite was prepared via a simple sol-gel method, using titanium *n*-butoxide and tetraethyl orthosilicate as the precursor. To assess the influence of thermal treatment on the microstructural and optical characteristics, the nanopowder was calcinated at temperatures of 400, 450, 500, 550, and 600 °C. The samples were analyzed using various techniques, such as X-ray diffraction (XRD), UV-Vis Diffuse Reflectance Spectra (DRS), and nitrogen adsorption-desorption isotherms (BET). The XRD patterns verify the formation of TiO_2 in the anatase phase, with an increase in crystallinity observed as the calcination temperature rises. The photocatalytic performance for phenol degradation was assessed in a batch reactor under simulated natural light, using a 26 W compact lamp. The synthesized TiO_2-SiO_2 composite (with a Ti/Si molar ratio of 95/5) exhibited the highest photocatalytic activity for phenol degradation, achieving a phenol degradation yield of 91.5% after 4 h of natural light irradiation. This result was obtained under calcination at 500 °C for 2 h.

Keywords: Photocatalyst, degradation of phenol, TiO_2-SiO_2, sol-gel method, composite.

1. INTRODUCTION

In recent years, advanced oxidation processes (AOPs) have garnered significant attention as promising technologies for phenol degradation and other persistent organic pollutants in wastewater. These processes offer a sustainable and energy-efficient pathway for the total oxidation of hazardous compounds, including aromatic hydrocarbons, pesticides, petroleum-derived substances, and volatile organic compounds. Among various photocatalytic materials, titanium dioxide (TiO_2) has emerged as a leading candidate owing to its high photocatalytic efficiency, chemical stability, non-toxicity, and low cost [1-5]. However, its practical application is hindered by inherent limitations such as a relatively wide band gap (3.2 eV) [6], which restricts visible-light absorption, and a low specific surface area [7].

To address these limitations, considerable research efforts have been directed toward modifying TiO_2 through metal and non-metal doping to narrow its band gap and enhance light absorption [8, 9]. In parallel, increasing the specific surface area has been identified as a critical factor in improving photocatalytic efficiency. Silica (SiO_2), a well-known adsorbent with high surface area and chemical stability, has been extensively utilized as a support material for TiO_2–SiO_2 composites. These composites have demonstrated superior photocatalytic activity compared to pristine TiO_2 in the degradation of various contaminants.

The incorporation of SiO_2 not only enhances the thermal stability of the anatase phase but also increases surface area and suppresses electron-hole recombination, thereby improving overall photocatalytic performance [10-12].

For instance, a study conducted by Diana Rakhmawaty Eddy et al. reported that TiO_2–SiO_2 composites exhibited enhanced catalytic performance, achieving a Cr(VI) degradation efficiency of up to 92.24%, significantly surpassing that of pure TiO_2 [6]. Moreover, the synthesis conditions, particularly the calcination temperature, play a vital role in determining the structural and photocatalytic properties of TiO_2–SiO_2 composites. The study by Yan Cheng and colleagues [13] focused on the influence of calcination temperature on the structure of TiO_2-SiO_2. The results showed that the calcination temperature has a significant effect on the crystal phase, which in turn greatly influences the photocatalytic activity. In this study, the phase transition temperature from anatase to rutile in the TiO_2-SiO_2 material reached up to 1200 °C. As reported by N.C. Horti and colleagues [14] calcination at 500 °C predominantly yields the anatase phase, which exhibits higher photocatalytic activity. In contrast, temperatures exceeding 600 °C lead to the formation of the rutile phase, which is generally less active.

In light of these considerations, the present study focuses on the synthesis of TiO_2–SiO_2 composites via the sol-gel method, with an emphasis on investigating the influence of calcination temperature on their structural characteristics and photocatalytic performance. Despite previous research highlighting the importance of calcination temperature, the underlying mechanisms affecting phase stability and activity remain unclear. Therefore, a systematic study is necessary to optimise synthesis conditions and enhance the material's efficiency. The findings aim to contribute to the advancement of efficient TiO_2–SiO_2–based photocatalysts for environmental remediation applications.

2. MATERIALS AND METHODS

2.1. Materials

Titanium n-butoxide (TNB, Merck 99%) and tetraethyl orthosilicate (TEOS, Merck 99%) were used as precursors for TiO_2 and SiO_2, respectively. Acetylacetone (AcAc, Merck 98%) as a gelation agent throughout the sol-gel process. Polyethylene glycol (PEG, Merck, average MW of 20,000) was used to increase viscosity, create porosity, and act as a dispersion medium for the mixture. Ethanol (EtOH, 99.5%) and distilled water were used in all experiments.

2.2. Synthesis TiO_2-SiO_2

The TiO_2-SiO_2 composite was prepared as follows: The TiO_2 solution was prepared by stirring TNB, EtOH (molar ratio 1:9), and ACAC at 80°C for 1 h, then cooling to room temperature for 30 minutes. The SiO_2 solution was prepared by stirring TEOS, EtOH, and HNO_3 (molar ratio 0.05:8:1) for 1 h. Subsequently, precise amounts of these two solutions were vigorously mixed at room temperature to obtain a mixture with a Ti/Si molar ratio of 95:5 (TS05). The resulting mixture was then aged for 40 h at room temperature, dried at 120 °C for 3 h, and calcined in air at temperatures ranging from 400 to 600 °C for 2 h.

2.3. Characterization of TiO_2-SiO_2

The characteristic structure of the TiO_2-SiO_2 composite material was determined by XRD using a D2 Phaser (Bruker) with Cu Kα radiation (λ = 0.154 nm). The crystal size was calculated using the Scherrer equation $t = \frac{0.9\lambda}{B.cos\theta}$, where t is the crystal size, λ is the wavelength, B is the full width at half maximum (FWHM) of the most intense peak, and θ is

the Bragg reflection angle. The optical properties of the material were investigated by UV–Vis diffuse reflectance spectroscopy (DRS). The spectra were recorded using a JASCO V-770 UV–Vis–NIR spectrophotometer at a scan rate of 400 nm/min, in the wavelength range of 220–850 nm, with a scan interval of 2 nm. The Brunauer–Emmett–Teller (BET) method, utilizing Quantachrome Instruments version 11.0, was used to measure the specific surface area.

2.4. Photocatalytic activity of TiO_2-SiO_2

The photocatalytic activity of the TiO_2-SiO_2 composite samples was evaluated based on the phenol degradation under laboratory conditions. A 500 mL reaction vessel contained 200 mL of phenol solution (initial concentration of 10 mg/L) and 200 mg of the catalyst sample. During the photocatalytic process, the mixture was stirred at room temperature and irradiated by a 26 W compact lamp (Natural light PT 2191-ExoTerra) with a wavelength range of 390 to 640 nm, with the highest intensity at 540 nm.

The lamp was positioned above the reaction vessel. Before irradiation, the mixture was stirred in the dark for 60 minutes to achieve adsorption equilibrium. The experiments were conducted for 4 h, and 5 mL samples were collected at specific intervals. Each sample was filtered through a 0.45 μm nylon filter to remove particles and mixed with 4-aminoantipyrine and potassium ferricyanide at pH 10 to form a coloured complex [15]. The mixture was then analyzed using a Hitachi UV-Vis spectrophotometer equipped with an ISSUV/VIS light source, covering a wavelength range of 400 to 600 nm. The degradation of phenol was monitored by its absorption peak at 510 nm.

3. RESULTS AND DISCUSSION

3.1. Characterization

The X-ray diffraction (XRD) patterns of the TS05 samples at calcination temperatures ranging from 400 to 600 °C are shown in Figure 1. All peaks in the diffraction pattern correspond to the anatase phase. Notably, the anatase phase appears at 400 °C, and even at 600 °C, no rutile phase is observed. This result indicates that the presence of SiO_2 has inhibited the phase transition from anatase to rutile [16].

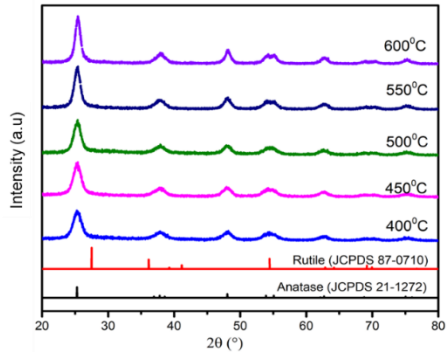

Figure 1. XRD spectra of synthesized TS05 with different calcination temperatures

Additionally, no peaks corresponding to SiO_2 appear in the X-ray diffraction pattern, indicating that SiO_2 exists in the material in an amorphous form [16, 17]. As the calcination temperature increases, the peaks become sharper, reflecting an increase in crystallinity and larger crystal size (Table 1). Specifically, at 400 °C, the crystal size is 4.9 nm, whereas at 600 °C, it increases to 7.7 nm.

Table 1. Crystallite size of TS05 samples at different calcination temperatures

Temperature (ºC)	Diameter (nm)
400	4.9
450	5.2
500	5.6
550	6.6
600	7.7

The UV-Vis absorption spectra of TS05 calcined at 400–600 °C for 2 h are shown in Figure 2. The spectra indicate strong absorption below 380 nm, attributed to the electron transition from the valence band to the conduction band [18]. Figure 2 presents the relationship between $(\alpha h\nu)^2$ and $h\nu$ (in eV), revealing that the band gap energy of the TS05 samples at 400, 450, 500, 550, and 600 °C is 3.17 eV, 3.17 eV, 3.18 eV, 3.25 eV, and 3.27 eV, respectively. The results indicate that the band gap value increases with calcination temperature.

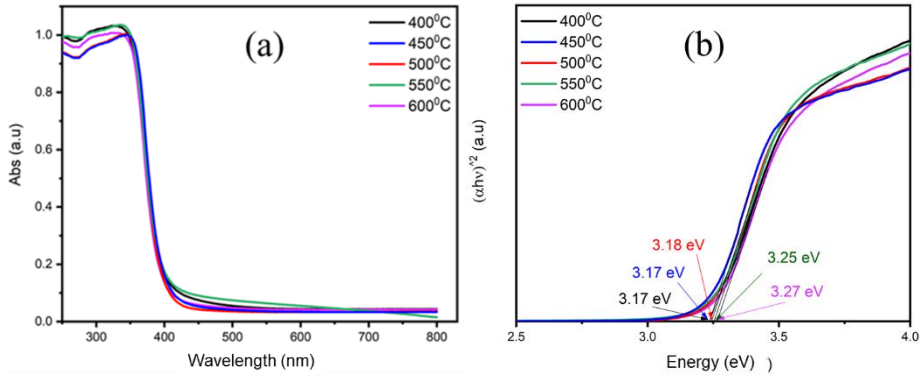

Figure 2. UV–Vis spectra of TS05 samples calcined at different temperatures

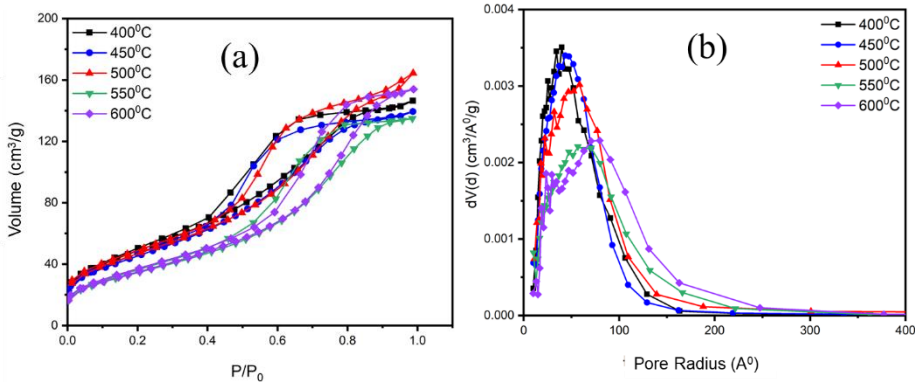

Figure 3. (a) Nitrogen adsorption–desorption isotherms and (b) BJH pore size distribution of TS05 samples calcined at 400–600 °C

Figure 3 presents the nitrogen adsorption-desorption isotherms and BJH pore size distribution curves of TS05 samples subjected to thermal treatment at temperatures ranging from 400 to 600 °C for 2 h. From Figure 3, the isotherm curves correspond to type IV according to the IUPAC classification. The hysteresis loops in the relative pressure range P/P_0=0.4−1.0 are attributed to capillary condensation, characteristic of mesoporous materials [8]. It can be observed that the TS05 sample calcined at 500 °C exhibits better nitrogen

adsorption capacity. Although its specific surface area slightly decreases, its pore diameter is significantly larger than the sample calcined at 400 °C. Additionally, the sample calcined at 600 °C has the largest pore diameter but a considerably lower specific surface area than that at 500 °C (Table 2).

Table 2. Specific surface area, pore volume, and pore diameter of TS05 samples calcined at 400–600 °C

Temperature (ºC)	S_{BET} (m^2/g)	V_{BJH} (cm^3/g)	D_{BJH} (A°)
400	180.97	0.24	40
450	168.54	0.23	44
500	170.93	0.26	59
550	127.80	0.22	57
600	130.67	0.28	80

3.2. Photocatalytic degradation

The phenol degradation efficiency of the TS05 samples at different calcination temperatures is shown in Figure 4. As the calcination temperature increases, the photocatalytic activity is also enhanced. However, beyond 500°C, the photocatalytic activity begins to decline. Specifically, after 4 h of irradiation, the remaining phenol concentration when degraded by TS05 samples calcined at 400, 450, 500, 550, and 600 °C is 3.27 (67.3%), 2.54 (74.6%), 0.85 (91.5%), 1.40 (86%), and 3.54 (64.6%) ppm, respectively.

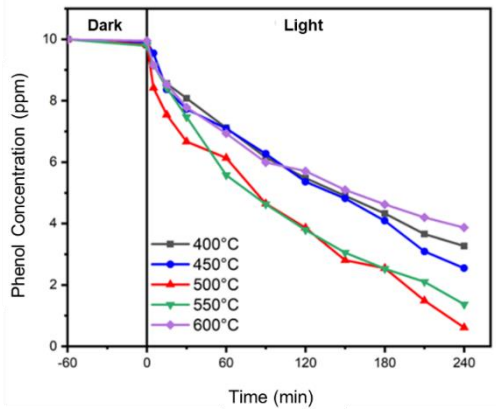

Figure 4. Phenol degradation by TS05 samples calcined at 400–600 °C

This phenomenon can be explained by the fact that at 400 °C and 450 °C, the anatase phase has formed; however, its low crystallinity results in lower photocatalytic activity [19]. At a calcination temperature of 500 °C, enhanced crystallinity leads to a reduction in structural defects, which in turn decreases the recombination rate of electrons and holes, thereby enhancing photocatalytic activity [9]. Additionally, at this temperature, the material exhibits a high specific surface area and large pore size, which further favours the photocatalytic process. However, at 550 °C, although the rutile phase is still absent, the reduction in specific surface area leads to a decline in photocatalytic activity. Although large pores are present at 600 °C, the enlarged crystal size and decreased specific surface area adversely affect the photocatalytic performance.

Figure 5 presents the kinetics of phenol degradation following two kinetic models for the TS05 catalyst calcined at 400–600 °C. The results indicate that the degradation rate of phenol follows the pseudo-first-order kinetic model more significantly than the pseudo-second-order model.

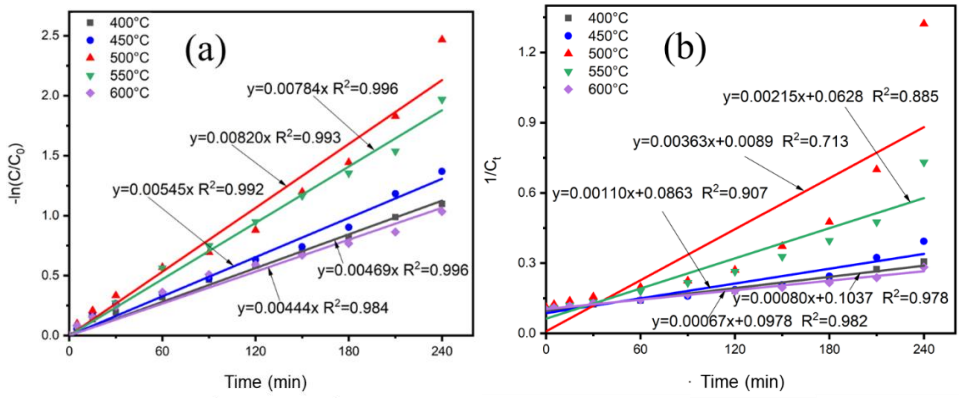

Figure 5. Kinetic Model for phenol removal a) Pseudo-first order and b) Pseudo-second order for TS05 samples at 400-600 °C

The rate constants for the two kinetic models are summarized in Table 3. A comparison of the R^2 values shows that the pseudo-first-order kinetic model has a higher R^2 value than the pseudo-second-order model. Specifically, for the TS05 catalyst calcined at 500 °C, the pseudo-first-order rate constant (k_I) is 0.00820 min^{-1} with an R^2 value of 0.993, whereas the pseudo-second-order rate constant (k_{II}) is 0.00363 mol^{-1} with an R^2 value of 0.713. These results indicate that the phenol degradation process of the TS05 catalyst at various calcination temperatures follows the pseudo-first-order kinetic model [20].

Table 3. Phenol degradation rate constants of TS05 at different calcination temperatures (pseudo-first- and second-order models)

Temperature (°C)	Pseudo-first-order kinetics		Pseudo-second-order kinetics	
	k_I x 10^2 (min^{-1})	R^2	k_{II} x 10^2 ($mol^{-1}.L.min^{-1}$)	R^2
400	0.469	0.996	0.080	0.978
450	0.545	0.992	0.110	0.907
500	0.820	0.993	0.363	0.713
550	0.783	0.996	0.215	0.885
600	0.444	0.984	0.067	0.982

Table 4. Worldwide studies on TiO_2–SiO_2 composite materials

Year	Material	Pollutant	S_{BET} (m^2/g)	Light source	Time (min)	Result (%)	References
2021	TiO_2-SiO_2	Methylene Blue	307.10	UV	60	96.8	[10]
2019	TiO_2-SiO_2	Methylene Blue	289.23	Visible	120	99.0	[17]
2019	TiO_2-SiO_2	Methyl Orange	95.96	Visible	120	92.0	[4]
2019	TiO_2-SiO_2	Brilliant blue	385.20	UV	170	99.8	[5]
2018	TiO_2-SiO_2	Phenol	352.00	Solar light	300	80.0	[21]
2016	TiO_2-SiO_2	2,4,5-trichlorophenol	224.97	-	180	97.5	[22]
2025	TiO_2-SiO_2	Phenol	170.90	Simulated natural light	240	91.5	This study

Table 4 presents studies worldwide on the photocatalytic degradation of pollutants in wastewater using TiO_2-SiO_2 materials. The results indicate that TiO_2-SiO_2 materials, with their large specific surface area, can effectively degrade organic pollutants present in wastewater. However, compared to other pollutants, phenol is more challenging to degrade. Therefore, research on using TiO_2-SiO_2 materials for phenol degradation is crucial. Notably, the result obtained in this study (91.5% phenol degradation after 240 minutes under simulated natural light) demonstrates high practical potential. These results support the development of high-performance TiO_2–SiO_2 photocatalysts for use in environmental treatment technologies.

4. CONCLUSION

This study highlights the influence of calcination temperature on the structural characteristics and photocatalytic activity of TiO_2–SiO_2 composites synthesized via the sol-gel method. The characteristic structure of the TiO_2-SiO_2 composite was determined through X-ray diffraction (XRD), UV-Vis Diffuse Reflectance Spectra (DRS), and nitrogen adsorption-desorption isotherms (BET). XRD analysis revealed that with the incorporation of SiO_2, the material maintained a single anatase phase even at a calcination temperature of 600 °C. The TS05 material calcined at 500 °C exhibited the highest phenol degradation efficiency, achieving 91.5%. These results provide a foundation for developing TiO_2-SiO_2 photocatalysts for environmental treatment applications.

Acknowledgement

We acknowledge Ho Chi Minh City University of Industry and Trade for supporting this study.

REFERENCES

1. Alwared A.I., Sulaiman F.A., Raad H., Al-Musawi T.J., and Mohammed N.A. - Ability of $FeNi_3/SiO_2/TiO_2$ nanocomposite to degrade amoxicillin in wastewater samples in solar light-driven processes, South African Journal of Botany **153** (2023) 195-202. https://doi.org/10.1016/j.sajb.2022.12.031.
2. Basavarajappa P.S., Patil S.B., Ganganagappa N., Reddy K.R., Raghu A.V., and Reddy C.V. - Recent progress in metal-doped TiO_2, non-metal doped/codoped TiO_2 and TiO_2 nanostructured hybrids for enhanced photocatalysis, International Journal of Hydrogen Energy **45** (13) (2020) 7764-7778. https://doi.org/ 10.1016/j.ijhydene.2019.07.241
3. Cetinkaya T., Neuwirthová L., Kutláková K.M., Tomášek V., and Akbulut H. - Synthesis of nanostructured TiO_2/SiO_2 as an effective photocatalyst for degradation of acid orange, Applied Surface Science **279** (2013) 384-390. https://doi.org/ 10.1016/j.apsusc.2013.04.121
4. Cui L., Song Y., Wang F., Sheng Y., and Zou H. - Electrospinning synthesis of SiO_2-TiO_2 hybrid nanofibers with large surface area and excellent photocatalytic activity, Applied Surface Science **488** (2019) 284-292. https://doi.org/ 10.1016/j.apsusc.2019.05.151
5. Dai H., Jun Z., Yin Y., Shao G., and Yu C. - Synthesis of Ag doped SiO_2-TiO_2 aerogels with nano-sized microcrystalline anatase structure through IL control, IOP Conference Series: Materials Science and Engineering **587** (2019) 012016. https://doi.org/10.1088/1757-899x/587/1/012016
6. Fan M., Fan G., Zhang G., and Zheng S. - Facile synthesis and kinetic mechanism of Ag-doped TiO_2/SiO_2 nanoparticles for phenol degradation under visible light

irradiation, Research on Chemical Intermediates **46** (2) (2019) 1127-1139. https://doi.org/ 10.1007/s11164-019-04023-8

7. Eddy D.R., Puri F.N., and Noviyanti A.R.J.P.C. - Synthesis and Photocatalytic Activity of Silica-based Sand Quartz as the Supporting TiO_2 Photocatalyst, **17** (2015) 55-58. https://doi.org/10.3390/app11199033
8. Guo N., Liang Y., Lan S., Liu L., Ji G., Gan S., Zou H., and Xu X. - Uniform TiO_2–SiO_2 hollow nanospheres: Synthesis, characterization and enhanced adsorption–photodegradation of azo dyes and phenol, Applied Surface Science **305** (2014) 562-574. https://doi.org/ 10.1016/j.apsusc.2014.03.136
9. Lin Y.T., Weng C.H., Hsu H.J., Lin Y.H., and Shiesh C.C. - The Synergistic Effect of Nitrogen Dopant and Calcination Temperature on the Visible-Light-Induced Photoactivity of N-Doped TiO_2, International Journal of Photoenergy **2013** (2013) 268723. https://doi.org/ 10.1155/2013/268723
10. Shchelokova E.A., Tyukavkina V.V., Tsyryatyeva A.V., and Kasikov A.G. - Synthesis and characterization of SiO_2-TiO_2 nanoparticles and their effect on the strength of self-cleaning cement composites, Construction and Building Materials **283** (2021) 122769. https://doi.org/ 10.1016/j.conbuildmat.2021.122769
11. Fatimah I., Prakoso N.I., Sahroni I., Musawwa M.M., Sim Y.L., Kooli F., and Muraza O. - Physicochemical characteristics and photocatalytic performance of TiO_2/SiO_2 catalyst synthesized using biogenic silica from bamboo leaves, Heliyon **5** (11) (2019) 02766. https://doi.org/ 10.1016/j.heliyon.2019.e02766
12. Utomo R.S.B., Sentanuhady J., and Muflikhun M.A. - TiO_2–SiO_2 nanocomposite via a novel sol-gel method with the addition of an energy monitoring device: Synthesized, characterization and anti-bacterial applications, Ceramics International **50** (13, Part A) (2024) 23367-23378. https://doi.org/ https://doi.org/10.1016/j.ceramint.2024.04.059
13. Cheng Y., Luoa F., Jianga Y., Lia F., and Wei C. - The effect of calcination temperature on the structure and activity of TiO_2/SiO_2 composite catalysts derived from titanium sulfate and fly ash acid sludge, Colloids and Surfaces A **554** (2018) 81-85. https://doi.org/10.1016/j.colsurfa.2018.06.032
14. Horti N.C., Kamatagi M.D., Patil N.R., Nataraj S.K., Sannaikar M.S., and Inamdar S.R. - Synthesis and photoluminescence properties of titanium oxide (TiO_2) nanoparticles: Effect of calcination temperature, Optik **194** (2019). https://doi.org/ 10.1016/j.ijleo.2019.163070
15. Medjor W.O., Wepuaka C.A., and Godwill S. - Spectrophotometric Determination of Phenol in Natural Waters by Trichloromethane Extraction Method after Steam Distillation, International Research Journal of Pure and Applied Chemistry **7** (3) (2015) 150-156. https://doi.org/ 10.9734/irjpac/2015/17160
16. Zhang L., Xing Z., Zhang H., Li Z., Wu X., Zhang X., Zhang Y., and Zhou W. - High thermostable ordered mesoporous SiO_2–TiO_2 coated circulating-bed biofilm reactor for unpredictable photocatalytic and biocatalytic performance, Applied Catalysis B: Environmental **180** (2016) 521-529. http://dx.doi.org/10.1016/j.apcatb.2015.07.002
17. Fatimah I., Prakoso N.I., Sahroni I., Musawwa M.M., Sim Y.L., Kooli F., and Muraza O. - Physicochemical characteristics and photocatalytic performance of TiO_2/SiO_2 catalyst synthesized using biogenic silica from bamboo leaves, Heliyon **5** (11) (2019) 02766. https://doi.org/10.1016/j.heliyon.2019.e02766
18. Fan M., Fan G., Zhang G., and Zheng S. - Facile synthesis and kinetic mechanism of Ag-doped TiO_2/SiO_2 nanoparticles for phenol degradation under visible light

irradiation, Research on Chemical Intermediates **46** (2) (2019) 1127-1139. https://doi.org/10.1007/s11164-019-04023-8

19. Shi Z., Yao S., and Sui C. - Application of fly ash supported titanium dioxide for phenol photodegradation in aqueous solution, Catalysis Science & Technology **1** (5) (2011) 817. https://doi.org/ 10.1039/c1cy00019e
20. Balakrishnan A., Gopalram K., and Appunni S. -Photocatalytic degradation of 2,4 dicholorophenoxyacetic acid by TiO_2 modified catalyst: kinetics and operating cost analysis, Environmental Science and Pollution Research, **28** (2021) 33331–33343. https://doi.org/10.1007/s11356-021-12928-4
21. Matos J., Llano B., Montana R., Poon P.S., and Hidalgo M.C. - Design of Ag/ and Pt/TiO_2-SiO_2 nanomaterials for the photocatalytic degradation of phenol under solar irradiation, Environment Science Pollution Residue International **25** (19) (2018) 18894-18913. https://doi.org/ 10.1007/s11356-018-2102-3
22. Zhang L., Xing Z., Zhang H., Li Z., Wu X., Zhang X., Zhang Y., and Zhou W. - High thermostable ordered mesoporous SiO_2–TiO_2 coated circulating-bed biofilm reactor for unpredictable photocatalytic and biocatalytic performance, Applied Catalysis B: Environmental **180** (2016) 521-529. https://doi.org/ 10.1016/j.apcatb.2015.07.002

TÓM TẮT

ẢNH HƯỞNG CỦA NHIỆT ĐỘ NUNG ĐẾN QUÁ TRÌNH TỔNG HỢP VẬT LIỆU TiO_2-SiO_2 COMPOSITE VÀ HIỆU QUẢ PHÂN HỦY PHENOL TRONG NƯỚC

Hồ Thị Ngọc Sương*

Trường Đại học Công Thương Thành phố Hồ Chí Minh

*Email: *suonghtn@huit.edu.vn*

Nghiên cứu nhằm đánh giá ảnh hưởng của nhiệt độ nung đến quá trình tổng hợp vật liệu TiO_2-SiO_2 composite và hiệu quả của chúng trong việc xử lý phenol trong dung dịch nước. Vật liệu TiO_2-SiO_2 được tổng hợp bằng phương pháp sol-gel với tiền chất ban đầu là titan *n*-butoxide và tetraethyl orthosilicate. Mẫu được nung ở nhiệt độ 400, 450, 500, 550 và 600 °C để nghiên cứu sự thay đổi về cấu trúc vi mô và tính chất quang học. Cấu trúc đặc trưng của vật liệu TiO_2-SiO_2 composite được xác định bởi phương pháp nhiễu xạ tia X (XRD), phổ phản xạ khuếch tán UV-Vis (DRS) và đường đẳng nhiệt hấp phụ- giải hấp phụ N_2 (BET). Kết quả XRD xác nhận sự hình thành pha anatase của TiO_2, với độ kết tinh tăng theo nhiệt độ nung. Hiệu quả quang xúc tác được đánh giá thông qua quá trình phân hủy phenol dưới ánh mô phỏng tự nhiên, sử dụng đèn compact 26 W. Mẫu composite TiO_2-SiO_2 có tỷ lệ mol Ti/Si là 95/5 và được nung ở 500 °C trong 2 giờ cho hiệu suất phân hủy phenol cao nhất, đạt 91,5% sau 4 giờ chiếu sáng.

Từ khóa: Xúc tác quang, phân hủy phenol, TiO_2-SiO_2, phương pháp Sol-gel, composite.